Optimization of Process Parameters in Powder-Mixed EDM

S. Tripathy and D. K. Tripathy

Abstract Electrical discharge machining (EDM) finds wide application all around the world for producing complex contour on very hard metals and alloys. It finds numerous applications in automobile, die making, aerospace, and electronic industries. Low volumetric material removal rate and reduced surface quality are few limitations of the process. Powder-mixed electro-discharge machining (PMEDM) is a novel advancement to EDM that has enhanced the machining capabilities of the process. The present chapter deals with the investigations on the effect of process variables like powder concentration (C_p), peak current (I_p), pulse-on-time (T_{on}), duty cycle (DC), and gap voltage (V_g) on output responses like material removal rate (MRR), tool wear rate (TWR), electrode wear ratio (EWR), surface roughness (SR), recast layer thickness (RLT), and microhardness (HVN) for PMEDM of H-11 hot work tool steel. The work material possesses excellent mechanical characteristics and finds huge application in various industries. Taguchi's L_{27} orthogonal array has been implemented to conduct the experiments using graphite powder-mixed dielectric with the copper tool. Single-objective optimization has been performed to determine the optimum set of input parameters. Analysis of variance (ANOVA) has been implemented to determine the effect of each process parameter and to establish the optimal setting of process parameters. Multi-objective optimization using technique for an order of preference by similarity to ideal solution (TOPSIS) was used to determine the optimum set of process variables to obtain maximum MRR and HVN with minimum TWR, EWR, SR and RLT simultaneously. Predicted results on verification with confirmation tests improve the preference values by 0.1021 with TOPSIS. The recommended settings of process parameters is found to be C_p = 6 g/l, I_p = 3 A, T_{on} = 200 µs, DC = 80% and V_g = 50 V from TOPSIS. The microstructures were examined with

S. Tripathy
Mechanical Engineering Department, Siksha 'O' Anusandhan (Deemed to be University), Bhubaneswar 751030, India

D. K. Tripathy (✉)
Indian Institute of Technology Kharagpur, Kharagpur, India
e-mail: dkt1946@yahoo.co.in

S. S. Pande and U. S. Dixit (eds.), *Precision Product-Process Design and Optimization*, Lecture Notes on Multidisciplinary Industrial Engineering,
https://doi.org/10.1007/978-981-10-8767-7_10

scanning electron microscope (SEM) to find the presence of surface defects and identify modifications on the surface.

Keywords PMEDM · Taguchi · TOPSIS · Material removal rate
Tool wear rate · Electrode wear ratio · Surface roughness · Recast layer thickness
Microhardness

1 Introduction

Novel manufacturing theory makes use of non-conventional sources of energy like light, sound, chemical, electrical, mechanical, ions and electrons. The technical and industrial advancement has led to the growth of very hard materials which are difficult to machine but are widely used in nuclear, aerospace and other industries. With the progress in the field of material science, advancement of latest metallic, ceramic materials and composite materials has been witnessed which possess excellent mechanical properties, thermal characteristics and electrical conductivity. Spark erosion machining techniques or non-traditional machining processes are used for machining such exotic materials. Non-traditional machining processes do not employ any conventional tools for material removal. The intricacy of the contour, size, requirement of product accurateness and high surface quality can be overcome by implementing non-traditional methods. Presently, non-conventional processes acquire infinite capabilities, but exhibit poor material removal rates. Enormous developments have taken place in the past few years for the improvement of MRR. With increase in removal rate, the cost efficiency of the process gets maximized, leading to greater application of non-traditional techniques for machining. Electrical discharge machining (EDM) is widely used for making tools, dies and parts with higher accuracy. Modern electric discharge machines have been established globally as a benchmark in manufacturing. They are proficient of machining geometrically complex components such as composites, superalloys, ceramics, heat-treated tool steels, heat-resistant steels, carbides etc. which find application in mould making industries, aeronautics, aerospace and nuclear industries. EDM has reached the recent fields of sports, optics, medicinal and surgical instruments, automotive and R&D areas.

The process of EDM came into existence in 1943, with its foundation in Moscow by the Russian scientists Boris and Natalya Lazarenko. The researchers reported that by immersing the electrodes in oil, steady sparks were generated than air. The phenomenon was inverted and controlled sparks were used for erosion. EDM machine was first developed during war by Lazarenkos. It was very useful for the erosion of metals like tungsten or tungsten carbide. Advancement for understanding the erosion phenomenon evolved in the 1950s. In 1960s, the growth in semiconductor industry endorsed substantial development in EDM machines with increased reliability that produced surfaces with superior quality. The development then led to the design of generators, automation, servo-control and robotics. During

1980s micro-machining using EDM gained a good deal of interest. The EDM process became globalized during this period. Subsequently, advancements to EDM emerged in the 1990s using neural networks, response surface methodology, fuzzy control, central composite design, Taguchi optimization etc. The research in this field is still in progress with innovative ideas of adding additives to the dielectric fluid like conductive powders, nano-sized particles, carbon nanotubes etc.

In EDM process the tool and workpiece material are separated by a small gap in the presence of a dielectric medium. High-frequency-controlled pulses are generated which creates a plasma channel due to the continuous movement of electrons and ions. The temperature in the discharge gap rises to a range of 8000–12,000 °C which causes melting and vaporization. PMEDM improves the process capabilities of EDM by producing surfaces with superior finish and less cracks. Adding fine powders to the dielectric decreases its insulating strength by increasing the inter-electrode gap. The removal of debris becomes easier in the presence of powders. On applying a voltage of 80–320 V an electric field is formed in the range of 10^5–10^7 V/m generating positive and negative charges on powder particles. This energizes powder particles and they move in zigzag manner forming clusters in the sparking area. Bridging occurs under the sparking area creating several discharges in a single pulse. The rapid sparking and erosion from the workpiece surface improve the machining rate. Widening of plasma channel produces stable sparks which form craters with improved surface finish. Material is removed from both the electrodes which combine with the powder particles and modifies the surface properties of the machined surface. Consequently, the MRR increases, TWR reduces and uniform sparks produce corrosion-resistant surfaces. The presence of abrasive powder changes the sparking pattern and improves the surface properties, increases the microhardness gets increased and micro-cracks get minimized. Added powders may be aluminium, chromium, graphite, silicon, titanium etc.

Pecas and Henriques (2008) reported that PMEDM process performance depends upon powder type, concentration, grain size, electrode area, constituents of the tool and workpiece material. Kumar et al. (2009) reviewed the outcome of mixing the dielectric fluid with various powders and additives. Assarzadeh and Ghoreishi (2013) implemented response surface methodology with desirability technique to model and optimize the process parameters during EDM of CK-45 die steel using Al_2O_3 powder-mixed dielectric to improve the MRR. Singh et al. (2012) investigated the effect of process parameters on SR for machining H-11 with the copper tool in the presence of Al powder in the dielectric. Negative polarity of the tool electrode reduced the SR. Talla et al. (2015) conducted multi-objective optimization of PMEDM using Taguchi, GRA and Principal Component Analysis (PCA) to control the process parameters. Lal (2015) performed multi-objective optimization with Taguchi-based GRA for wire EDM. Sidhu et al. (2014) reported the optimal process setting for machining of three types of MMCs using PMEDM. MRR, TWR, SR and surface integrity were examined to determine the significant process parameters. The responses were jointly optimized using technique for order of preference by similarity to ideal solution (TOPSIS) and optimal process conditions were recognized. Singh et al. (2015) examined the outcome of adding graphite

powder to the dielectric on the surface properties of superalloy Super Co 605. The results showed that an optimization between microhardness and surface finish can be achieved by this method of machining. Batish and Bhattacharya (2012) studied the material migration occurring between electrode and powder-suspended dielectric fluid for enhancing the surface properties in terms of microhardness for H-11 and H-13 steels. Aluminium, copper, graphite and tungsten powders were added to kerosene, EDM oil, and refined mineral oil as dielectric. Sidhu et al. (2014) optimized MRR, TWR, SR and surface integrity for three different metal matrix composites using TOPSIS and the ranking was done as per the severity of surface defects. Gadakh (2012) applied TOPSIS method for solving multiple criteria optimization problem in wire electrical discharge machining (WEDM) and obtained the most suitable set of process parameters.

From the available literature it is evident that several researchers have reported results using different powders mixed during EDM, but performance characteristics of H-11 during PMEDM needs investigation. The quality of the machined component is defined by various output characteristics such as MRR, TWR, SR, recast layer thickness, microhardness obtained on the machining surface etc. Thus, investigating the significance of the process variables in relation to the output performance characteristics becomes vital. Therefore the problem of PMEDM can be considered as a multi-objective optimization problem. The aim of this study is to obtain a single-optimal setting of various input parameters to obtain a single-output characteristic as a whole. Multi-attribute decision-making techniques like TOPSIS have not yet been used to find the optimal setting during PMEDM of H-11. The present work is a stride in this direction. Taguchi design of experiments is used to conduct the experiments using an L_{27} orthogonal array. An effort has been made to find an optimal set of process variables by using multi-objective optimization using TOPSIS to get maximum MRR and minimum TWR, EWR, SR, RLT and maximum HVN by adding graphite powder to the dielectric in different concentrations. ANOVA has been used to create a relationship among the significant input parameters on the output responses. A comparative study for the EDM and PMEDM surface characteristics has been done using scanning electron microscope. The optimal parameter setting obtained from Taguchi and TOPSIS can be used for quality improvement in industrial applications involving PMEDM.

2 Materials and Methods

The machines, materials and design of experiment technique adopted for the estimation of output responses are highlighted in this section. The procedure used for optimization has also been presented in this section.

2.1 EDM Machine Set-up

The electric discharge machine, model ELECTRONICA-ELECTRAPULS PS 50ZNC has been used for the experiments. Commercial-grade EDM oil has been used as a dielectric fluid. To facilitate the generation of a rectangular form of current pulses for discharging, dielectric fluid was energized by "Current Pulse Generator" and associate controller. The current and voltage waveforms were recorded on a "Digital Storage Oscilloscope". Figure 1 shows the machine used in the present study.

Working tank of the machine had a capacity of 300 L for the circulation of dielectric fluid. The powder particles were required to be added in different

Fig. 1 EDM machine used for the experiment

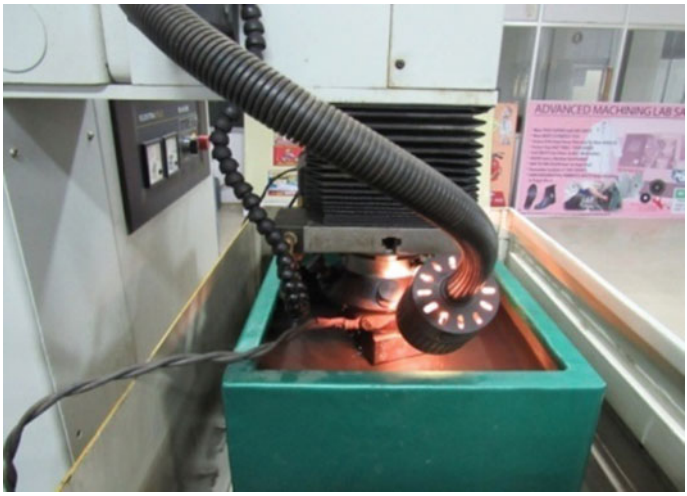

Fig. 2 PMEDM setup (Tripathy and Tripathy 2017b, c)

concentrations for which changing the entire dielectric fluid and removing the powder particles from the circulating system would have been difficult. The existing circulation system might have choked due to the presence of powders and debris. To minimize the cost, avoid the wastage of dielectric and for effective use of powder particles, a separate machining tank has been designed with a capacity of 20 L. It consists of a machining tank to perform the operation placed in the working tank of EDM. A workpiece fixture assembly was placed in it to hold the workpiece. The machining tank was filled up with the dielectric fluid. A pump was installed to ensure proper distribution of powder in dielectric fluid. To avoid the powder from settling down, a stirring arrangement was installed. Each run was carried out for a time duration of 15 min. The setup of the tank is shown in Fig. 2.

2.2 Selection of Materials

The mechanical properties and composition of the workpiece and tool material used for the present experiment have been discussed in this section.

2.2.1 Workpiece Material

H-11 hot work tool steel is the workpiece material. This steel possesses very high strength, abrasion resistance, wear resistance, compressive strength, hardenability, toughness and it is not susceptible to hot cracking. The presence of chromium in the H-11 steel resists oxidization whereas molybdenum prevents corrosion in

Table 1 Mechanical properties of H-11 steel

Properties	H-11
Density	7.81 g/cm^3
Modulus of elasticity	210 GPa
Poisson's ratio	0.30
Yield strength	1650 MPa
Ultimate tensile strength	1990 MPa
Specific gravity	7.8
Melting temperature	1427 °C
Thermal conductivity	42.2 W/mK
Hardness	55 HRC

Table 2 Chemical composition of H-11 steel

Constituent	C	Si	Mn	P	S	Cr	Mo	Co	Cu	V	Fe
% Composition	0.39	1	0.5	0.03	0.02	4.75	1.1	0.01	0.01	0.5	Balance

non-oxidizing environments. The mechanical properties of the H-11 steel are given in Table 1. Applications of H-11 is found in aircraft components, structural use, die casting dies, extrusion tooling, forging dies, piercing tools, hot work punches, tool holders, ejector pins etc. The properties cause a great challenge during machining by conventional methods. The chemical composition of this material as obtained by glow discharge-optical emission spectrometer is given in Table 2. Each surface of the workpiece and tool were machined using CNC-milling machine to get smooth mirror-like surfaces. The electrodes were subjected to surface grinding for proper contact and alignment of surfaces during machining. The dimension of the workpiece used for this EDM operation was 120 × 60 × 25 mm.

2.2.2 Tool Material

Electrolytic copper electrode (99.9%) has been used as the tool electrode material. A square tool of dimension 20 × 20 × 60 mm has been used to perform the machining operation. The mechanical properties of the tool material are given in Table 3. The work material was mounted on the T-slot table and positioned at the desired place and clamped. The electrode was clamped and its alignment was

Table 3 Properties of tool electrode material

Electrode material	Density (g/cc)	Specific heat (J/kg/K)	Thermal conductivity (W/mK)	Electrode resistivity (μΩ)	Hardness BHN
Electrolytic copper	8.9	386	388	1.69	48

checked. The machining was performed for time duration of 15 min. Finally the essential power switches were switched 'ON' for operating the desired machine settings.

2.3 Process Parameters

The process parameters chosen for the present research work are powder concentration (C_p), peak current (I_p), pulse on time (T_{on}), duty cycle (DC) and gap voltage (V_g) to study their effect on output parameters e.g. material removal rate (MRR), tool wear rate (TWR), electrode wear ratio (EWR), surface roughness (SR), recast layer thickness (RLT) and microhardness (HVN) based upon the significant effect on the EDM and PMEDM process and the extensive literature review presented. The methodology to assess the performance characteristics are discussed below.

2.3.1 Material Removal Rate

High material removal rate is the most desirable output response for any machining process which leads to increased productivity. After each machining operation, the workpiece material was taken out and weighed to find out the weight loss. Weight of the workpiece before and after the experiment was measured using an electronic balance with a least count of 0.001 g. The time duration of each experimental run was recorded using a digital stop watch. From the weight loss obtained, the material removal rate was calculated for different experimental runs. MRR is calculated using the volume loss from the workpiece material as cubic millimetre per minute (mm^3/min). The MRR is expressed as:

$$\begin{aligned} \text{MRR } \left(\text{mm}^3/\text{min}\right) &= \frac{\text{Wear weight of the work piece}}{\rho \times \text{time}} \\ \text{MRR} &= w_i - w_f/\rho * T \end{aligned} \tag{1}$$

where w_i and w_f are initial and final weights of the workpiece before and after the machining process, ρ is density of the workpiece material and T is the machining time in minutes.

2.3.2 Tool Wear Rate

The tool material for machining is selected based upon the principle that the material should have low resistance to electricity and high melting point. The tool electrode was taken out and weighed after each machining operation to find out the

weight loss. Weight of the tool before and after the experiment was measured to determine the tool wear rate. The TWR is expressed as:

$$\begin{aligned} \text{TWR } \left(\text{mm}^3/\text{min}\right) &= \frac{\text{Wear weight of the tool}}{\rho \times \text{time}} \\ \text{TWR} &= t_i - t_f/\rho * T \end{aligned} \tag{2}$$

where t_i and t_f are initial and final weights of the tool before and after the machining process, ρ is density of the tool and T is the machining time in minutes.

2.3.3 Electrode Wear Ratio

The electrode wear ratio is dependent on the material removal rate and the tool wear rate. Lower EWR is desirable to enhance the productivity of the process. EWR can be defined as "the ratio of weight of the electrode wear to the weight of the workpiece wear after machining" and is expressed as:

$$\begin{aligned} \text{EWR } (\%) &= \frac{\text{``Wear weight of the tool''}}{\text{``Wear weight of the work piece''}} \times 100 \\ \text{EWR} &= w_t/w_w * 100 \end{aligned} \tag{3}$$

where w_t and w_w are the wear weights of the tool and workpiece material measured after the machining operation is carried out in relation to the TWR and MRR.

2.3.4 Surface Roughness

Larger is the vertical deviation, rougher is the surface. The surface roughness is measured based upon various statistical descriptors out of which centre line average method is mostly used. SR is the arithmetic mean of the deviations from the mean line. The expression for R_a is given as:

$$R_a = \left(\frac{1}{L}\right) \int_0^L |y(x)| \mathrm{d}x \tag{4}$$

where, L is the sampling length, y is the profile curve sampled by the set of N points and x is the profile direction. The roughness of the surface was measured using a surface roughness tester (Talysurf, Rank Taylor Hobson, England, Model-Surtronic S-100 series).

2.3.5 Recast Layer Thickness

During the machining process, a small amount of material gets re-solidified after being melted due to the refrigeration effect of the dielectric fluid. This layer is known as the recast layer. Material transfer also takes place from the powder suspended in the dielectric fluid and also from the electrode to the machined surface. Beyond this layer lies the heat-affected zone and the base material. In order to find out the structural features present below the machined surface and the distribution of cracks in the recast layer, specimens were cut from the machined surface in a traverse direction and were then mounted for metallographic studies. The recast layer thickness was measured using a scanning electron microscope (FESEM, model: Supra 55, Zeiss, Germany) for all the experiments by taking three sets of readings for a particular experiment and considering the average of the three values as the average recast layer thickness.

2.3.6 Microhardness

After the metallographic analysis, the samples were measured for hardness in a microhardness tester (LM 247AT of LECO) under a load of 10 mgf. The purpose of obtaining the microhardness of the material before and after machining was to examine the change in hardness and its effect on the machining surface due to the addition of the powder particles during machining. The microhardness was measured at three different locations and the average value was considered to be the microhardness of the machined specimen.

2.4 Design of Experiments

Taguchi's technique uses a philosophy and methodology to improve the quality of the process and minimizes the cost involved to carry out the process by optimizing the product design using statistical concepts. The effect of various machining process parameters such as concentration of powder (C_p), peak current (I_p), pulse on time (T_{on}), duty cycle (DC) and gap voltage (V_g) on various output responses like material removal rate (MRR), tool wear rate (TWR), electrode wear ratio (EWR), surface roughness (SR), recast layer thickness (RLT) and microhardness (HVN) on H-11 hot work tool steel was investigated using Taguchi's parameter design and Analysis of variance (ANOVA) helps to determine the statistically significant parameters affecting the responses. Predicted results obtained by Taguchi's technique were verified through confirmatory tests for validation and minimization of errors. Taguchi prescribes the use of orthogonal arrays (OA) for experiments. The design of experiments involves the assignment of important and influencing parameters to appropriate columns in the array with the use of linear graphs or triangular tables as suggested by Taguchi. The use of array in the design provides

almost identical experimental runs. The most important stage in the DOE lies in the selection of control factors and their levels. The results are further analysed to establish the optimal condition for a product or process, estimation of the contribution of individual parameters affecting the response, and to determine the optimum response under the best condition. The best condition may be determined by analysing the behaviour of minimum effects of each of the parameters which provides the trend of each parameter and its influence on the process. ANOVA is applied to the results which help to determine the percentage contribution of each parameter for a stated level of confidence. The ANOVA table suggests which parameters need to be controlled. Taguchi suggests two ways to carry out the complete analysis. In the first case, the results of a single run or the average of repetitive runs are analysed through main effects plot and ANOVA (raw data analysis). The second approach uses signal-to-noise (S/N) ratio to the previous steps. The S/N ratio is a concurrent quality metric linked to the loss function. As S/N ratio maximizes, the loss associated gets minimized. S/N ratio provides the robust set of operating conditions for the process. S/N ratio is defined as "the ratio of the mean of the signal to the standard deviation of the noise". It is denoted by 'η' and it has the unit of dB. The present analysis involves the use of Taguchi's orthogonal array to conduct the experiments and the optimum setting is obtained by analyzing the main effect plot aided by the raw data analysis aided by S/N data analysis followed by ANOVA. Based upon the trial experiments and extensive literature survey, the significant machining parameters taken into consideration are concentration of powder (C_p), peak current (I_p), pulse on time (T_{on}), duty cycle (DC) and gap voltage (V_g) and their effect on the output responses has been investigated. Three sets of experimental runs have been performed at each condition. The control factors were selected based on the literature survey and some preliminary investigations. L_{27} Taguchi's orthogonal array was used for the experiments as shown in Table 4.

2.4.1 Signal-to-Noise Ratio

Establishment of the loss function with its appropriate k value and to use it as a figure of merit is not easy and cost-effective. Thus, the loss function is transformed

Table 4 Selection of levels for the factors

Factors with symbol and units	Levels		
	Level 1	Level 2	Level 3
Concentration of graphite powder 'C_p' (g/L)	0	3	6
Peak current 'I_p' (A)	3	6	9
Pulse on time 'T_{on}' (μs)	100	150	200
Duty cycle 'DC' (%)	7	8	9
Gap voltage 'V_g' (V)	30	40	50

to S/N ratio. S/N ratio being a concurrent statistics uses two or more characteristics of distribution and converts them into a single figure of merit. A higher value of S/N ratio implies that signal is much higher than the random effect of noise factors. The equations for calculating S/N ratios for "lower-the-better (LB), higher-the-better (HB) and nominal-the-best (NB)" type of characteristics are:

$$\text{LB: S/N Ratio} = -10\log_{10}\left[\frac{1}{n}\sum_{i=1}^{n} y_i^2\right] \tag{5}$$

$$\text{HB: S/N Ratio} = -10\log_{10}\left[\frac{1}{n}\sum_{i=1}^{n} y_i^{-2}\right] \tag{6}$$

$$\text{NB: S/N Ratio} = -10\log_{10}\left[\frac{1}{n}\sum_{i=1}^{n} (y_i - y_0)^2\right] \tag{7}$$

where

y sample mean
z standard deviation for the number of observations in each trial.
y_o nominal value of the characteristic

2.4.2 Selection of Orthogonal Array and Parameter Assignment

Selection of orthogonal array depends on the number of controllable parameters, their interactions with each other, and the number of levels to be selected. The number of controllable parameters with their levels considered in the present work is shown in Table 4. The minimum DOF required for the experiment are the sum of all the degrees of freedom of the factors. In the present experimental investigation, five three-level factors are considered for the study. As per Taguchi's experimental design philosophy, a set of three levels assigned to each parameter has two degrees of freedom. Thus, total DOF of the experiment becomes 10. The OA to be used should have more than 10 DOF. Hence, an L_{27} OA was chosen which has 27 trials and 26 DOF, assuming the interaction effect of process parameters negligible as shown in Table 5. The additional DOF may be used to measure the random error. Twenty-seven experiments each were conducted for three different powders mixed with the dielectric fluid using Taguchi's experimental design methodology, repeating each experiment three times. The designs, plots, and analysis have been carried out with MINITAB 15 software.

Table 5 Taguchi's L_{27} standard orthogonal array

Column no.	1	2	3	4	5
Run	C_p	I_p	T_{on}	DC	V_g
1	1	1	1	1	1
2	1	1	1	1	2
3	1	1	1	1	3
4	1	2	2	2	1
5	1	2	2	2	2
6	1	2	2	2	3
7	1	3	3	3	1
8	1	3	3	3	2
9	1	3	3	3	3
10	2	1	2	3	1
11	2	1	2	3	2
12	2	1	2	3	3
13	2	2	3	1	1
14	2	2	3	1	2
15	2	2	3	1	3
16	2	3	1	2	1
17	2	3	1	2	2
18	2	3	1	2	3
19	3	1	3	2	1
20	3	1	3	2	2
21	3	1	3	2	3
22	3	2	1	3	1
23	3	2	1	3	2
24	3	2	1	3	3
25	3	3	2	1	1
26	3	3	2	1	2
27	3	3	2	1	3

2.4.3 Analysis of Variance

Analysis of variance (ANOVA) was performed to determine the significant effect of process parameters on performance characteristics. The main effect plots for factors show the trend of the influence of factors toward the process. The importance of process variables with respect to output responses helps to determine the optimum set of parameters using ANOVA from Minitab15 software. Various steps involved in the analysis are:

Step 1: Total of all results (T):

$$T = \sum_{i=1}^{n} \sum_{j=1}^{R} y_{ij}, \tag{8}$$

where, y_{ij} is the value of the characteristic in the ith trial and jth repetition.

Step 2: Correction Factor (C.F.):

$$\text{C.F.} = T^2/N, \text{ where } N \text{ is the total number of experiments i.e. } 3 \times 27 = 81. \tag{9}$$

Step 3: Total sum of squares (SS_T):

$$\text{SS}_T = \sum_{i=1}^{n} \sum_{j=1}^{R} y_{ij} - \text{C.F.} \tag{10}$$

Step 4: Sum of squares of parameter A (SS_A):

$$\text{SS}_A = \left[\frac{A(1)^2}{N_{A1}} + \frac{A(2)^2}{N_{A2}} + \frac{A(3)^2}{N_{A3}} \right] - \text{C.F.} \tag{11}$$

where, N_{A1}, N_{A2} and N_{A3} are the number of experiments with parameter A at levels 1, 2 and 3, respectively. The sums of squares for all the factors are calculated similarly.

Step 5: Error sum of squares:

$$\text{SS}_e = \text{SS}_T - (\text{Summation of sum of squares of all the parameters}) \tag{12}$$

where, e stands for the error.

Step 6: Degrees of freedom:

$$\text{Total DOF} = (\text{total number of trials} - 1) = (R \times n - 1) = 80 \tag{13}$$

DOF of each parameters = (Number of levels of each parameter − 1) = 2
The DOF for all parameters are calculated in the similar way.

Step 7: Mean square of variance (V):

$$V_A = \text{Variance due to parameter } A = \frac{\text{SS}_A}{\text{fA}} \tag{14}$$

Variance for the other parameters is obtained in the similar manner.

Step 8: Percentage contribution (P):
P_A = Percentage contribution of parameter A towards mean of the response

$$P_A = \left(\frac{\mathrm{SS}_A}{\mathrm{SS}_T}\right) \times 100 \tag{15}$$

Similarly, the percentage contribution of all other parameters is calculated.

Step 9: F-ratios:
The F-ratio is defined as the ratio of variance due to a parameter and due to its error.

$$F_A = \frac{V_A}{V_e} \tag{16}$$

The F-ratio is calculated for all the parameters in the similar manner.

2.5 *Multi-objective Optimization*

Taguchi's experimental philosophy is focused on optimizing the process parameters in the perspective of a single quality criterion which does not give sufficient idea about the influence on other performance characteristics involved. The performance of the product is evaluated by various response parameters. Taguchi technique cannot solve a multi-response optimization problem. Hence, multi-objective optimization techniques are implemented wherein the quality characteristics are optimized and the results for the best levels are obtained. Taguchi technique is often combined with multi-objective optimization techniques to switch a multi-decision-making technique to a single-objective optimization problem. The decision maker assigns different priority weights to the responses basing upon their relative importance.

2.5.1 Technique for Order of Preference by Similarity to Ideal Solution (TOPSIS)

The present study focuses on finding the most suitable set of process variables for PMEDM using TOPSIS to obtain maximum MRR and HVN along with minimum TWR, EWR SR, and RLT with graphite powder-mixed dielectric. The optimum set of input parameters should be identified to improve the machining process for performance characteristics and surface quality and improve the machining characteristics of H-11 tool steel. Analysis of variance (ANOVA) helps to identify the statistically significant input parameters that affect the performance parameters.

TOPSIS is a capable multi-objective decision-making tool for solving complex decision-making problems in manufacturing domain where number of criteria, alternatives and their interactions play a significant role and their simultaneous effect influences the process to a great deal. TOPSIS uses preference grades with ranking order to find the most suitable set of input variables for the performance measures. TOPSIS can be used suitably for solving any type of decision-making problems. TOPSIS is a multi-optimization technique used to find the best alternative from a finite set. The technique is based upon the principle that the chosen criteria should have the shortest distance from the positive ideal solution and greatest distance from the negative ideal solution, the best solution being the closest to the ideal solution. The steps involved in carrying out the procedure of TOPSIS are:

Step 1 The decision matrix is the first step of TOPSIS which consist of 'n' attributes and 'm' alternatives and is represented as (Tripathy and Tripathy 2017b, c):

$$D_m = \begin{bmatrix} x_{11} & x_{12} & x_{13} & \cdots & \cdots & x_{1n} \\ x_{21} & x_{22} & x_{23} & \cdots & \cdots & x_{2n} \\ x_{31} & x_{32} & x_{33} & \cdots & \cdots & x_{3n} \\ \vdots & \vdots & \vdots & \ddots & \ddots & \vdots \\ \vdots & \vdots & \vdots & \ddots & \ddots & \vdots \\ x_{m1} & x_{m2} & x_{m3} & \cdots & \cdots & x_{mn} \end{bmatrix} \tag{17}$$

where x_{ij} is the performance of ith alternative with respect to jth attribute.

Step 2 Normalized matrix is obtained by the following expression:

$$r_{ij} = \frac{x_{ij}}{\sqrt{\sum_{i=1}^{m} x_{ij}^2}} \quad j = 1, 2, \ldots, n. \tag{18}$$

Step 3 The weight of each attribute was assumed to be w_j (j = 1, 2, …, n). Weighted normalized decision matrix $V = [v_{ij}]$ may be obtained as:

$$V = w_j r_{ij} \tag{19}$$

where, $\sum_{j=1}^{n} w_j = 1$.

Step 4 The most suitable and least suitable solutions may be obtained from the following expressions:

$$\begin{aligned} V^+ &= \left\{ \left(\sum_i^{\max} v_{ij} | j \in J \right), \left(\sum_i^{\min} | j \in J | i = 1, 2, \ldots m \right) \right\} \\ &= \left\{ v_1^+, v_2^+, v_3^+, \ldots, v_n^+ \right\} \end{aligned} \tag{20}$$

$$V^- = \left\{ \left(\sum_i^{\max} v_{ij} | j \in J \right), \left(\sum_i^{\min} | j \in J | i = 1, 2, \ldots m \right) \right\} = \left\{ v_1^-, v_2^-, v_3^-, \ldots, v_n^- \right\} \quad (21)$$

Step 5 The separation of alternatives from positive ideal solution is given by:

$$S_i^+ = \sqrt{\sum_{j=1}^n \left(v_{ij} - v_j^+ \right)^2}, \quad i = 1, 2, \ldots m \quad (22)$$

The separation of alternatives from negative-ideal solution is given by:

$$S_i^- = \sqrt{\sum_{j=1}^n \left(v_{ij} - v_j^- \right)^2}, \quad i = 1, 2, \ldots m \quad (23)$$

Step 6 The relative closeness of the alternative to the ideal solution is calculated and expressed as:

$$P_i = \frac{S_i^-}{S_i^+ + S_i^-} \quad i = 1, 2, \ldots m \quad (24)$$

Step 7 The P_i value was ranked in descending order to identify the set of alternatives having the preferred solutions.

Preference value of alternatives can be calculated from their nearness to ideal solution. The ratio of negative ideal separation measure divided by the sum of negative ideal separation measure and the positive ideal separation measure gives the relative closeness. The normalized matrix, weighted normalized decision matrix, separation of alternatives from positive and negative ideal solutions and preference values for TOPSIS for the runs with the ordered rankings are presented in Tables 25, 26, 27 and 28 respectively. The most suitable value of performance measure is the one which is close to the ideal solution of the performance measure and has the maximum preference value with the highest rank.

3 Results and Discussions

Experimental results obtained by varying the chosen set of input parameters for the selected output responses have been presented in this section. The discussion of the obtained results and the variations in their behaviour has also been detailed in the present section.

3.1 Experimental Results

Experiments were conducted using Taguchi's L_{27} orthogonal array. The results are represented in Table 6.

3.2 Effect of Process Parameters on Response Characteristics

The influence of input parameters on response characteristics has been highlighted in the present section. The variation of the output response with each input parameter has been discussed with the help of respective graphs.

Table 6 L_{27} experimental design with response variables

Run	C_p	I_p	T_{on}	DC	V_g	Avg MRR	Avg TWR	Avg EWR	Avg SR	Avg RLT	Avg HVN
1	0	3	100	7	30	2.564	0.0172	0.6718	3.8	13.8	784
2	0	3	100	7	40	2.649	0.0194	0.735	4.1	14.4	778
3	0	3	100	7	50	2.735	0.0224	0.8216	4.5	15.2	786
4	0	6	150	8	30	4.529	0.0277	0.6118	4.87	18.76	795
5	0	6	150	8	40	5.470	0.0307	0.5614	5.45	19.24	804
6	0	6	150	8	50	6.666	0.0367	0.5505	5.86	19.76	798
7	0	9	200	9	30	9.401	0.3895	4.1430	6.5	20.58	809
8	0	9	200	9	40	10.256	0.4868	4.7471	7.47	21.6	802
9	0	9	200	9	50	10.940	0.5243	4.7928	9.2	22.24	811
10	3	3	150	9	30	2.87	0.0123	0.429	2.48	22.6	833
11	3	3	150	9	40	3.54	0.0134	0.380	2.97	25.67	862
12	3	3	150	9	50	3.97	0.0152	0.383	3.42	25.31	841
13	3	6	200	7	30	4.42	0.0171	0.387	4.16	28.86	884
14	3	6	200	7	40	6.638	0.0186	0.2813	4.37	26.74	898
15	3	6	200	7	50	8.54	0.0192	0.224	4.82	29.2	876
16	3	9	100	8	30	9.26	0.0235	0.254	5.74	31.19	905
17	3	9	100	8	40	9.82	0.0261	0.266	6.41	34.42	929
18	3	9	100	8	50	11.04	0.0291	0.2639	6.72	37.64	976
19	6	3	200	8	30	5.56	0.0349	0.628	1.64	24.36	845
20	6	3	200	8	40	6.41	0.0378	0.5897	1.92	26.63	878
21	6	3	200	8	50	7.23	0.0398	0.5506	2.23	27.59	859
22	6	6	100	9	30	8.37	0.0448	0.5363	2.62	29.21	893
23	6	6	100	9	40	8.858	0.0463	0.523	2.94	32.49	904
24	6	6	100	9	50	11.23	0.0496	0.441	3.36	35.93	916
25	6	9	150	7	30	11.86	0.0586	0.494	3.82	36.2	941
26	6	9	150	7	40	12.07	0.0753	0.624	4.48	37.56	966
27	6	9	150	7	50	12.54	0.0880	0.7018	5.24	38.92	952

3.2.1 Effect of Process Parameters on Material Removal Rate

The goal of machining is high material removal and low tool wear. The MRR is the volume of material being removed per minute during machining. Experimental results show that machining without powder increases the MRR as I_p and T_{on} increase whereas the TWR, SR and RLT increase hampering the surface texture. Addition of powder in varying concentration modifies the surface properties. It causes a decrease in insulating strength of the dielectric fluid while increasing the inter-electrode gap making the removal of debris easier. Rapid sparks are generated due to the bridging effect which erodes material faster from the workpiece and increases the machining rate. Widening of plasma channel generates consistent sparks creating shallow craters on the machined region with superior surface finish. When graphite powder is added in C_p of 0 g/L, the MRR varies in a range of 2.564–10.940 mm^3/min. When C_p increases to 3 g/L, the MRR shows slight increase from 2.87–11.04 mm^3/min. Further increase of C_p to 6 g/L improves the MRR in a range of 5.56–12.54 mm^3/min. The variation of MRR with the input parameters is shown in Fig. 3a–e. As the I_p increases, the MRR increases significantly as more thermal energy is produced in the discharge channel as the electrical power increases. As T_{on} increases, the MRR slightly decreases and then tends to increase with the increase in discharge energy and heat transferred to the section. The decrease in MRR is due to the constant flushing pressure which is not sufficient to remove the molten material causing redeposition on the surfaces. The abrasive property of the powder promotes makes the removal of debris easier. The discharge gap distance increases with V_g, which consequently increases the material deposition on the surface which may be minimized under proper flushing conditions.

3.2.2 Effect of Process Parameters on Tool Wear Rate

Tool wear rate is determined as the volumetric material removed per minute during machining from the tool surface. The main aim of machining should be less tool wear for more amount of material removed from the workpiece surface. When no powder is added to the dielectric, the tool wear varies within a range of 0.0172–0.5243 mm^3/min. With the increase in C_p, the tool wear rate shows reduction. The TWR shows an increase with further increase in the concentration of powder to compensate for the more amount of MRR. With more MRR, TWR also shows an increase irrespective of the concentration of powder added to the dielectric as shown in Fig. 4a. More amount of MRR is observed while the I_p is more. Thus, more TWR occurs when more MRR is achieved with increased I_p. With the addition of 0 g/L of graphite powder, the maximum TWR is 0.5243 mm^3/min which reduces to a maximum value of 0.1517 mm^3/min when 3 g/L of graphite powder. On addition of 6 g/L of graphite powder, the maximum TWR reaches to a value of 0.2341 mm^3/min which is higher than that achieved with a C_p of 3 g/L. When graphite powder is added to the dielectric, more amount of carbon gets deposited on both the tool and workpiece surface. The resolidified layer on the

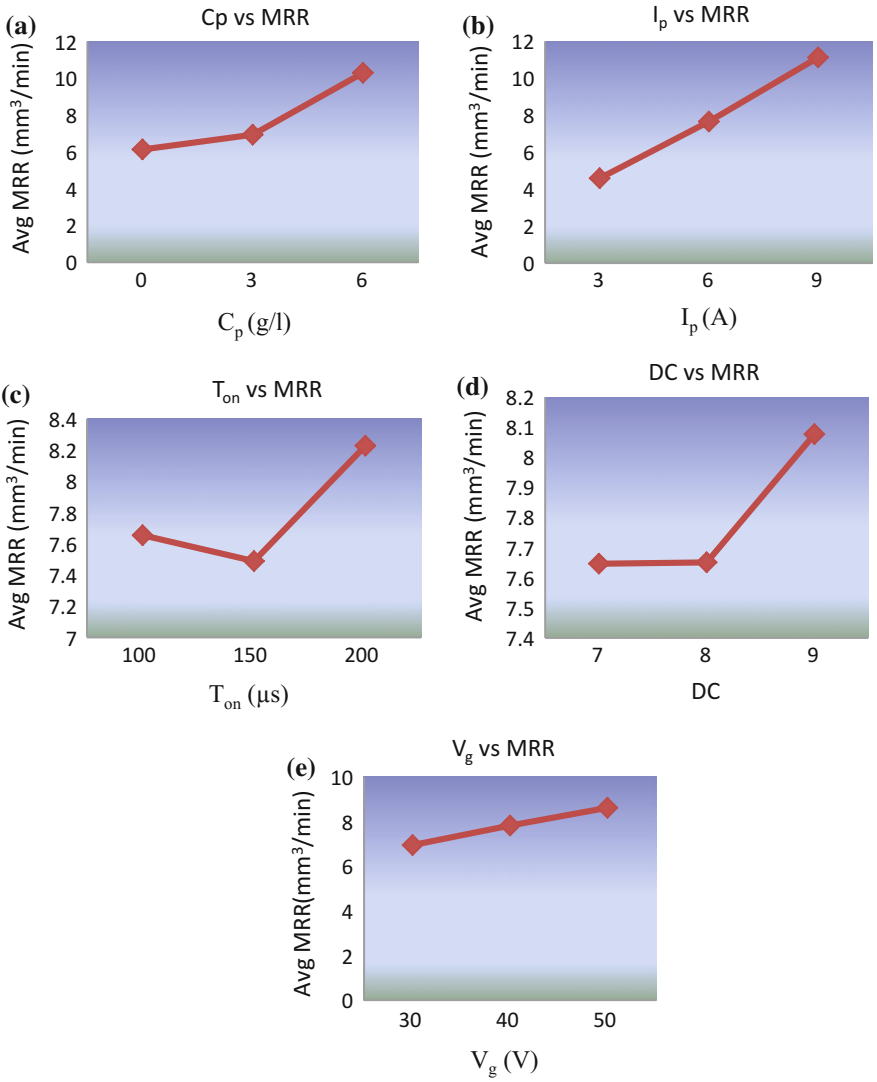

Fig. 3 Variation of MRR with process parameters (Tripathy and Tripathy 2017b, c)

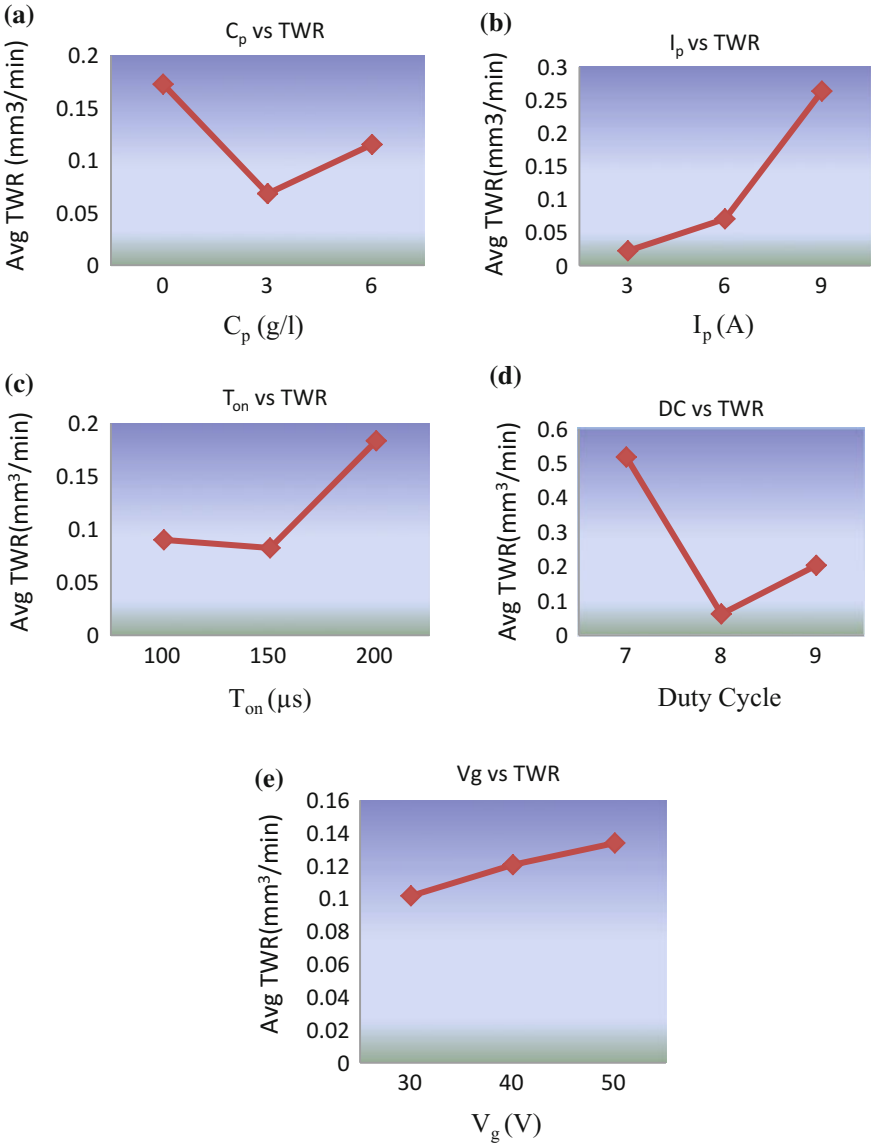

Fig. 4 Variation of TWR with process parameters (Tripathy and Tripathy 2017b, c)

workpiece leads to the recast layer formation and causes damage to the workpiece surface. Increased carbon content can be removed with proper flushing, which if insufficient would lead to increased TWR. Figure 4b–e show that with the increase in current and pulse on time the MRR and the TWR consequently increase due to the increased thermal energy in the discharge channel. This phenomenon is observed irrespective of the increase in the concentration of powders. With the increase in duty cycle, the tool wear rate increases as the material removal rate also show an increase due to the rapid ejection of molten material. The tool wear rate also shows an increase with the increase in gap voltage as the increased discharge gap distance increases the deposition of material on the machined surface and to perform the erosion of material from this deposited layer, the TWR shows an increase. With proper flushing conditions, higher machining rates can be achieved.

3.2.3 Effect of Process Parameters on Electrode Wear Ratio

The characteristic of a perfect tool should be the potential of removing maximum material from the workpiece with the capability to resist self-erosion. When the machining is performed without addition of powder, the increase in I_p and T_{on}, increases the EWR. With the addition of powder, the EWR decreases which is the result of less tool wear with more material removal from the workpiece. Figure 5a–e show that with the increase in concentration of powder-mixed to the dielectric, the EWR tends to decrease initially up to C_p of 3 g/L of powder but on increasing the C_p to 6 g/L, the EWR increases to a value much lower than that achieved with a C_p of 0 g/L. The nature of the variation of EWR can be related to the machining rates achieved by the addition of powder to the dielectric. The maximum value of EWR at 0, 3 and 6 g/L is 4.7928, 1.2777 and 1.711% respectively. With the increase in I_p, the EWR increases for graphite powder-mixed dielectric. This is because of the more thermal energy generated in the discharge channel. The EWR shows variation in relation to the amount of material removed and the corresponding TWR for the maximum amount of material removed from the workpiece. With the increase in T_{on}, the EWR shows a decrease followed by a significant increase with the further increase of T_{on}. With the increase in DC, the EWR tends to decrease initially followed by a significant rise with the increase in DC. This is because of the fact that for a C_p of 3 g/L, the amount of material removed from workpiece is less than that with a C_p of 6 g/L, with a subsequent increase in TWR. Hence, the EWR initially decreases, then increases due to the rapid ejection of molten material with the increase in DC. With the increase in V_g, the EWR increases due to the increase in discharge gap distance which leads to more amount of material deposition on the top surface of the workpiece leading to the increase in TWR for the required amount of MRR in presence of proper flushing.

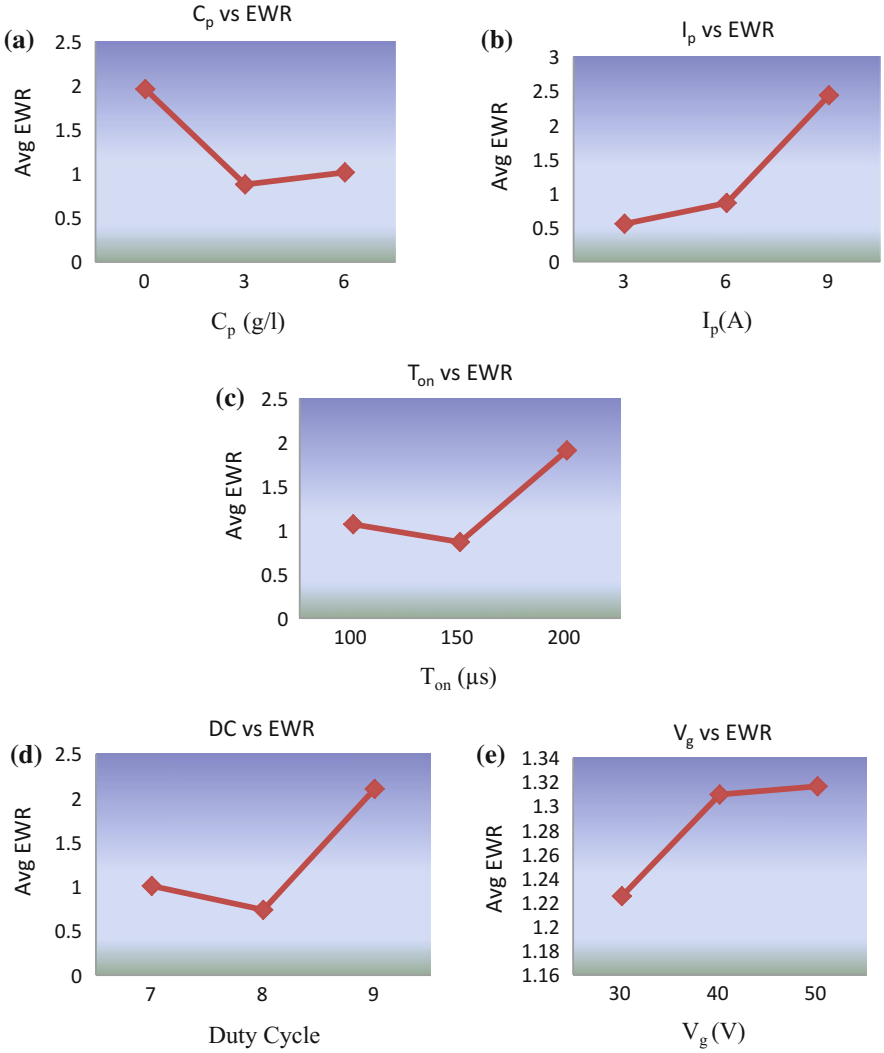

Fig. 5 Variation of EWR with process parameters

3.2.4 Effect of Process Parameters on Surface Roughness

The SR during PMEDM depends on size of the crater and variation of recast layer. From the experimental results, it can be seen that the roughness of the surface varies within a range of 3.8–6.19 μm without addition of powder. On addition of graphite powder in a C_p of 3 g/L, the SR lies between 1.94 and 5.65 μm. As the C_p increases to 6 g/L, the SR varies in a range of 2.41–6.19 μm. Influence of input parameters on SR is shown in Fig. 6a–e. With the rise in pulse current, the SR increases as the large dispersive energy cause impulsive forces and violent sparks which result in formation of large craters leading to the increase of SR as shown in Fig. 6b. Complete flushing does not occur during the pulse—off-time which increases the SR due to resolidification. Adding foreign particles in proper size and quantities reduce the SR during machining. With the increase in T_{on}, more heat is transferred to the section causing more material removal and increased SR. During PMEDM, the plasma flushing efficiency increases which improves the surface texture. Material deposition and carbide formation increases the SR. SR increases with increase in V_g as increased discharge gap distance minimizes the effect of induced energy at the workpiece surface thus increasing the deposition on the machined surface producing increased SR.

3.2.5 Effect of Process Parameters on Recast Layer Thickness

RLT increases with the increase in machining rate. It can be seen from Fig. 7a–e that increase in I_p increases the RLT. The temperature on the surface thus rises to the melting temperature consequently increasing the amount of material removed. Since the dielectric fluid does not get sufficient time to remove the molten material, the RLT increases. Increasing the C_p also increases the RLT as more amount of material is removed in presence of powder particles and redeposition occurs if flushing is insufficient which tends to increase the RLT. With the increase in T_{on}, the amount of heat transferred to the section increases. Adding graphite powder while machining and the breakdown of the dielectric fluid increases the carbon content. During PMEDM, as the T_{on} increases, the RLT tends to increase followed by reduction as the process becomes stable with the increase in discharge rate. Increase in DC, increases the RLT by a subsequent decrease which is due to the conduction of heat into the workpiece with a decrease in discharge duration. The abrasive effect of the powder particles decreases the RLT with the increase in DC. Increase in V_g increases the RLT due to the increase in discharge gap distance, which reduces the effect of induced energy at the workpiece and increases material deposition.

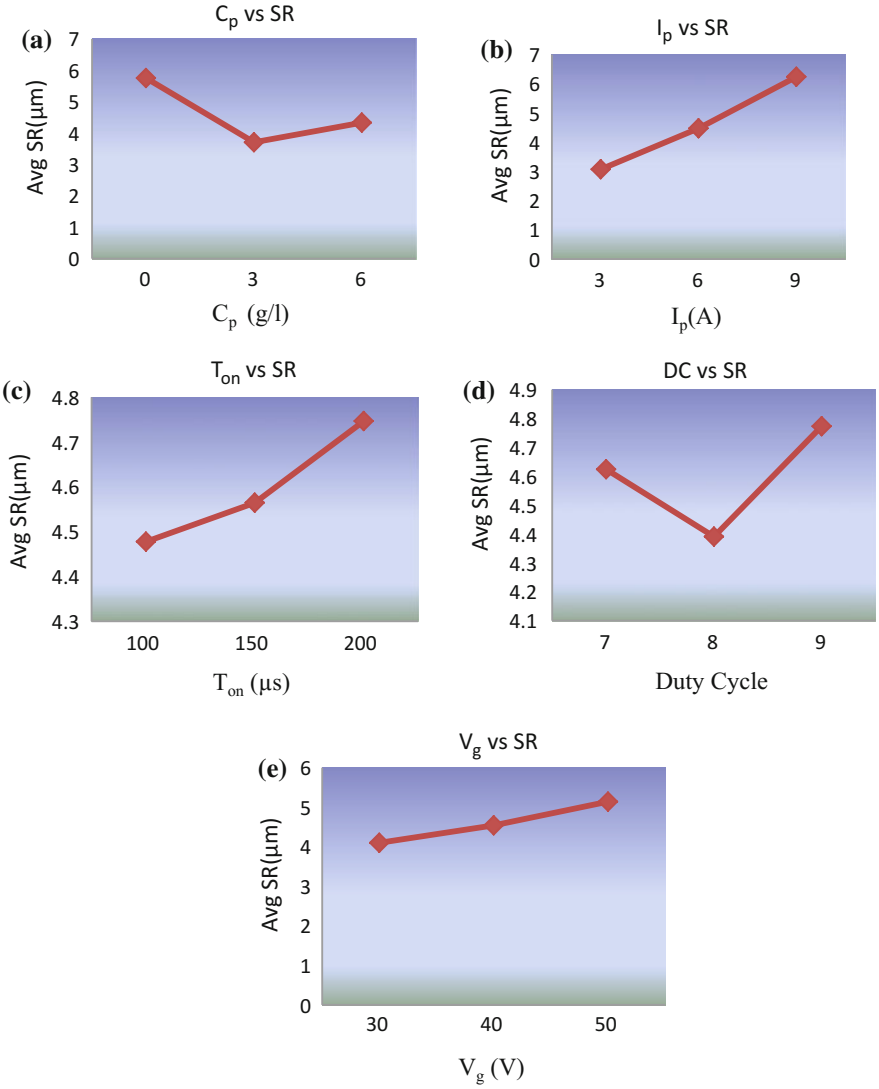

Fig. 6 Variation of SR with process parameters (Tripathy and Tripathy 2017b, c)

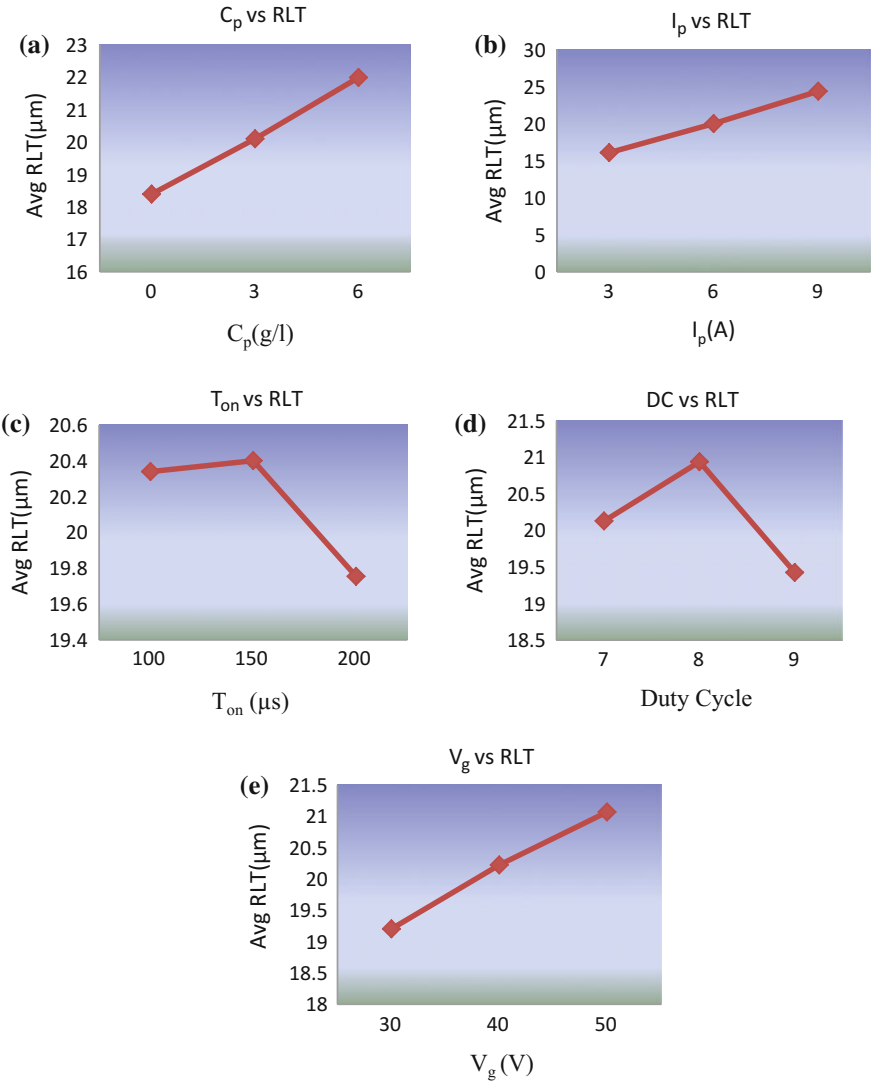

Fig. 7 Variation of RLT with process parameters (Tripathy and Tripathy 2017b, c)

3.2.6 Effect of Process Parameters on Microhardness

The microhardness of the parent material before machining has been found to be 621. The microhardness of the material after PMEDM was nearly double of the value before machining. It can be observed from Fig. 8a–e that the increase in C_p and I_p, increase the HVN values appreciably. Melting and deposition phenomenon increase the HVN. It may be observed that the surface quality is increased with the increase in HVN. The HVN increases while machining without the addition of powder with the increase in the values of I_p and T_{on} as high current increases the pulse energy. As the discharge column expands at higher pulse on time more heating of the surface occurs which releases the stresses and lowers the HVN at higher pulse on time. Increase in DC decreases the HVN as a consequence of the decrease in HVN with the variation of T_{on}. As V_g increases HVN also increases due to improper flushing of the debris during the no spark condition.

3.3 ANOVA Results for the Output Responses

The ANOVA results of each output response have been discussed in this section. The optimum set of process parameters has also been identified using the main effect plots for S/N ratio and means.

3.3.1 Analysis of Variance for Material Removal Rate

From the main effect plots shown in Fig. 9, the influence of different factors on the process can be visualized. The significance of the process variables in relation to MRR was investigated and the optimum combination of parameters was determined from the ANOVA analysis presented in Tables 7 and 8 respectively. MRR being higher-the-better type of quality characteristic, from the response curves as shown in Fig. 9a, it can be revealed that the third level of parameters of C_p, third level of I_p, third level of T_{on}, third level of DC and third level of V_g may offer maximum MRR. It may be noticed that the parameters C_p, I_p, T_{on} and V_g show similar trend of variation in both the main effect plots whereas DC shows the best value in the third level from the main effect plot of means and second level as a best value from the main effect plot for S/N ratio. In order to arrive at the final optimal setting, the relative contribution of the mean and S/N values has been considered from the ANOVA table.

The relative contribution of DC towards mean value of MRR (0.36%) is lower than that of S/N ratio (2.02%). Therefore, considering the level corresponding to the higher relative contribution, the optimum combination of input parameters for best MRR is the third level of parameters of C_p, third level of I_p, third level of T_{on}, second level of DC and third level of V_g which has been obtained at the main effect plot of S/N ratio.

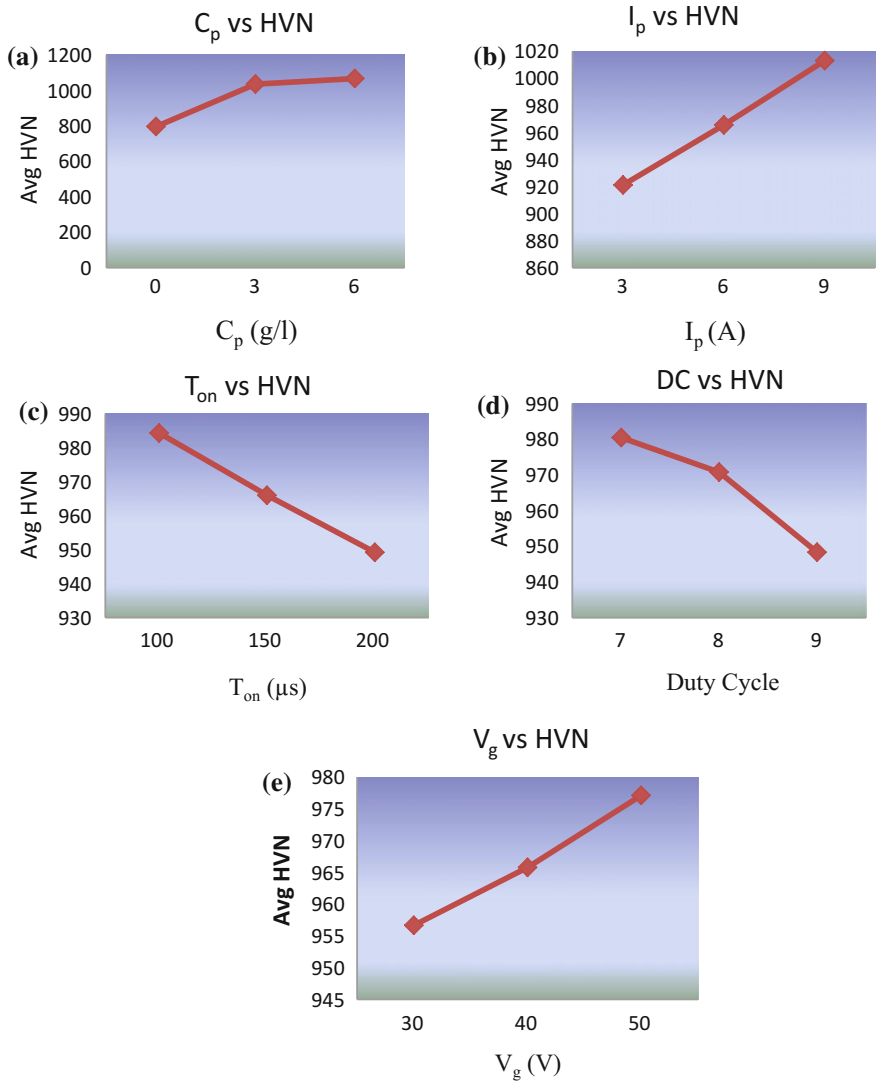

Fig. 8 Variation of HVN with process parameters

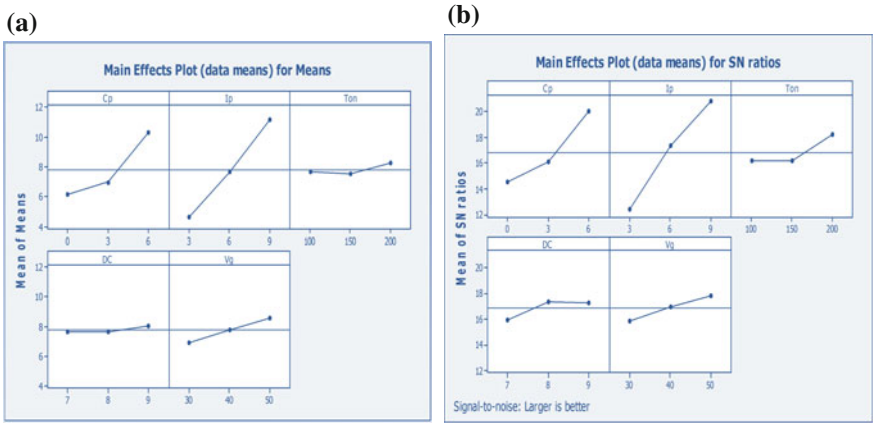

Fig. 9 Main effect plot for means and S/N ratio of material removal rate. **a** Main effect plot for means of MRR (Tripathy and Tripathy 2017a). **b** Main effect plot for S/N ratio of MRR

Table 7 ANOVA table for means of MRR

Source	DF	Seq SS	Adj SS	Adj MS	*F*	*P*	*P* (%)
C_p	2	87.870	87.870	43.9349	119.53	0.000	28.97
I_p	2	193.092	193.092	96.5458	262.66	0.000	63.68
T_{on}	2	2.711	2.711	1.3554	3.69	0.048	0.89
DC	2	1.099	1.099	0.5496	1.5	0.254	0.36
V_g	2	12.570	12.57	6.285	17.1	0.000	4.14
Error	16	5.881	5.881	0.3676			
Total	26	303.222					

S = 0.6063, R-Sq = 98.1%, R-Sq(adj) = 96.8%

Table 8 ANOVA table for S/N ratio of MRR

Source	DF	Seq SS	Adj SS	Adj MS	*F*	*P*	*P* (%)
C_p	2	145.504	145.504	72.752	191.26	0.000	27.64
I_p	2	323.339	323.339	161.67	425.02	0.000	61.42
T_{on}	2	23.662	23.662	11.831	31.1	0.000	4.49
DC	2	10.635	10.635	5.317	13.98	0.000	2.02
V_g	2	17.180	17.180	8.59	22.58	0.000	3.26
Error	16	6.086	6.086	0.38			
Total	26	526.406					

S = 0.6167, R-Sq = 98.8%, R-Sq(adj) = 98.1%

Table 9 Response table for means of MRR

Level	C_p	I_p	T_{on}	DC	V_g
1	6.134	4.586	7.655	7.646	6.941
2	6.938	7.654	7.489	7.650	7.820
3	10.299	11.132	8.228	8.076	8.611
Delta	4.165	6.546	0.740	0.430	1.671
Rank	2	1	4	5	3

The response table for all the process parameters is shown in Table 9. The ranks are based upon delta statistics that evaluate relative magnitude of effects.

3.3.2 Analysis of Variance for Tool Wear Rate

Figure 10 represents the influence of different factors on the process. The significance of the process variables in relation to TWR was investigated and the optimum combination of parameters was determined from the ANOVA analysis presented in Tables 10 and 11 respectively.

TWR being lower-the-better type of quality characteristic, the tendency of deviation of the response curves as shown in Fig. 10 demonstrate that the optimal set of parameters for TWR is the second level of parameters of C_p, first level of I_p, second level of T_{on}, second level of DC, and first level of V_g. The response table for all the process parameters is shown in Table 12.

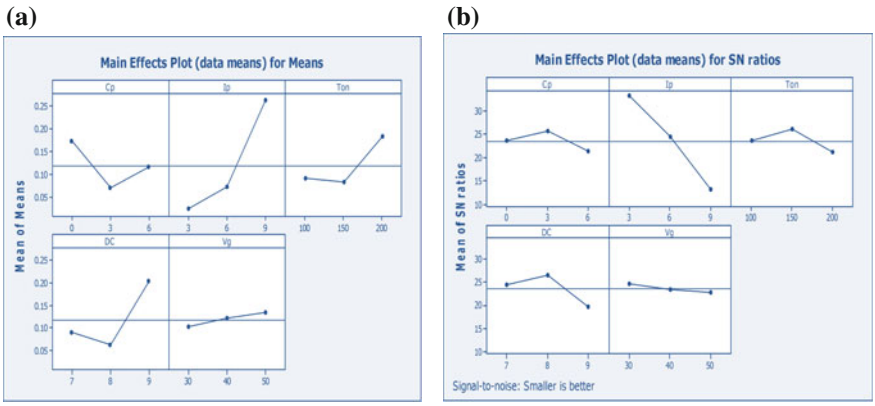

Fig. 10 Main effect plot for means and S/N ratio of tool wear rate. **a** Main effect plot for means of TWR (Tripathy and Tripathy 2017a). **b** Main effect plot for S/N ratio of TWR

Table 10 ANOVA table for means of TWR

Source	DF	Seq SS	Adj SS	Adj MS	*F*	*P*	*P* (%)
C_p	2	0.0493	0.0493	0.0247	35.68	0.000	9.57
I_p	2	0.2923	0.2923	0.1461	211.4	0.000	56.74
T_{on}	2	0.0571	0.0571	0.0286	41.34	0.000	11.09
DC	2	0.1005	0.1005	0.0503	72.72	0.000	19.51
V_g	2	0.0047	0.0047	0.0024	3.42	0.058	0.919
Error	16	0.01106	0.01106	0.00069			
Total	26	0.515157					

S = 0.02629, R-Sq = 97.9%, R-Sq(adj) = 96.5%

3.3.3 Analysis of Variance for Electrode Wear Ratio

Figure 11 shows the influence of different factors on the process. The significance of the process variables in relation to EWR was investigated and the optimum combination of parameters was determined from the ANOVA analysis presented in Tables 13 and 14 respectively.

EWR being lower-the-better type of quality characteristic, the trend of deviation of the response curves as shown in Fig. 11 demonstrate that the optimal set of parameters for EWR is the second level of parameters of C_p, first level of I_p, second level of T_{on}, second level of DC and first level of V_g. The response table for all the process parameters is shown in Table 15.

3.3.4 Analysis of Variance for Surface Roughness

Figure 12 demonstrates the influence of different factors on the process. The significance of the process variables in relation to SR has been investigated and the optimum combination of parameters was determined from the ANOVA analysis presented in Tables 16 and 17 respectively.

Table 11 ANOVA table for S/N ratio of TWR

Source	DF	Seq SS	Adj SS	Adj MS	*F*	*P*	*P* (%)
C_p	2	85.29	85.29	42.645	26.54	0.000	3.699
I_p	2	1840.29	1840.29	920.145	572.73	0.000	79.83
T_{on}	2	116.89	116.89	58.444	36.38	0.000	49.68
DC	2	220.35	220.35	110.175	68.58	0.000	9.558
V_g	2	16.74	16.74	8.371	5.21	0.018	7.11
Error	16	25.71	25.71	1.607			
Total	26	2305.26					

S = 1.268, R-Sq = 98.9%, R-Sq(adj) = 98.2%

Table 12 Response table for means of TWR

Level	C_p	I_p	T_{on}	DC	V_g
1	0.1727	0.0223	0.0901	0.0906	0.1016
2	0.0682	0.0706	0.0823	0.0621	0.1206
3	0.1151	0.2632	0.1836	0.2034	0.1338
Delta	0.1045	0.2408	0.1012	0.1413	0.0322
Rank	3	1	4	2	5

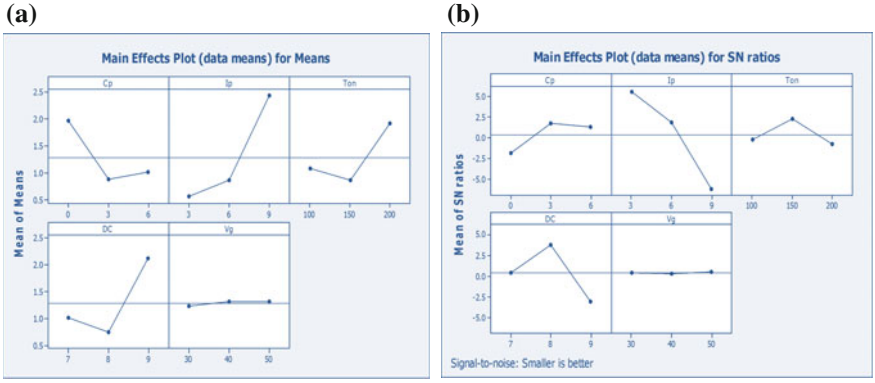

Fig. 11 Main effect plot for means and S/N ratio of electrode wear ratio. **a** Main effect plot for means of EWR. **b** Main effect plot for S/N ratio of EWR

Table 13 ANOVA table for means of EWR

Source	DF	Seq SS	Adj SS	Adj MS	F	P	P (%)
C_p	2	6.2531	6.253	3.1265	86.21	0.000	15.57
I_p	2	18.3438	18.343	9.1719	252.91	0.000	45.66
T_{on}	2	5.5277	5.5277	2.7638	76.21	0.000	13.76
DC	2	9.4095	9.4095	4.7047	129.73	0.000	2.34
V_g	2	0.0462	0.0462	0.0231	0.64	0.542	0.115
Error	16	0.5803	0.5803	0.0362			
Total	26	40.1606					

S = 0.1904, R-Sq = 98.6%, R-Sq(adj) = 97.7%

SR being lower-the-better type of quality characteristic, the tendency of deviation of the response curves demonstrate that the optimal set of parameters for SR is the second level of parameters of C_p, first level of I_p, first level of T_{on}, second level of DC and first level of V_g as shown in Fig. 12. The response table for all the process parameters is shown in Table 18.

Table 14 ANOVA table for S/N ratio of EWR

Source	DF	Seq SS	Adj SS	Adj MS	F	P	P (%)
C_p	2	71.56	71.56	35.78	19.15	0.000	7.08
I_p	2	644.33	644.33	322.167	172.41	0.000	63.81
T_{on}	2	49.41	49.41	24.704	13.22	0.000	4.89
DC	2	214.38	214.38	107.190	57.36	0.000	21.23
V_g	2	0.16	0.16	0.081	0.04	0.958	0.015
Error	16	29.90	29.90	1.869			
Total	26	1009.74					

S = 1.367, R-Sq = 97%, R-Sq(adj) = 95.2%

Table 15 Response table for means of EWR

Level	C_p	I_p	T_{on}	DC	V_g
1	1.9594	0.5549	1.0704	1.0086	1.2252
2	0.8766	0.8599	0.8676	0.7383	1.3094
3	1.0145	2.4358	1.9126	2.1037	1.3161
Delta	1.0828	1.8809	1.0450	1.3654	0.0909
Rank	3	1	4	2	5

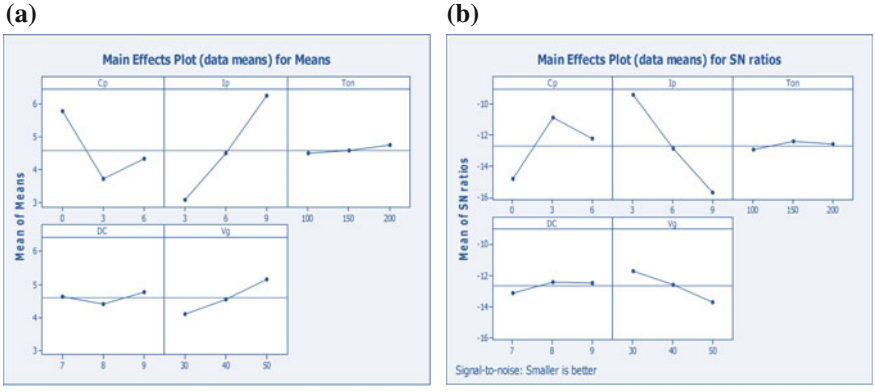

Fig. 12 Main effect plot for means and S/N ratio of surface roughness. **a** Main effect plot for means of SR (Tripathy and Tripathy 2017a). **b** Main effect plot for S/N ratio of SR

3.3.5 Analysis of Variance for Recast Layer Thickness

Figure 13 shows the influence of different factors on the process. The significance of the process variables in relation to RLT has been investigated and the optimum combination of parameters was determined from the ANOVA analysis presented in Tables 19 and 20 respectively.

Table 16 ANOVA table for means of SR

Source	DF	Seq SS	Adj SS	Adj MS	F	P	P (%)
C_p	2	19.7174	19.7174	9.8687	79.15	0.000	26.96
I_p	2	45.4767	45.4767	22.7383	182.55	0.000	62.2
T_{on}	2	0.3391	0.3391	0.1695	1.36	0.285	0.463
DC	2	0.6681	0.6681	0.3341	2.68	0.099	0.913
V_g	2	4.9155	4.9155	2.4577	19.73	0.000	6.723
Error	16	1.9929	1.9929	0.1246			
Total	26	73.1096					

S = 0.3529, R-Sq = 97.3%, R-Sq(adj) = 95.6%

Table 17 ANOVA table for S/N ratio of SR

Source	DF	Seq SS	Adj SS	Adj MS	F	P	P (%)
C_p	2	72.595	72.595	36.2973	187.75	0.000	26.31
I_p	2	178.867	178.867	89.4333	462.59	0.000	64.84
T_{on}	2	1.125	1.125	0.5626	2.91	0.084	0.407
DC	2	2.449	2.449	1.2245	6.33	0.009	0.887
V_g	2	17.713	17.713	8.8564	45.81	0.000	6.421
Error	16	3.093	3.093	0.1933			
Total	26	275.842					

S = 0.4397, R-Sq = 98.9%, R-Sq(adj) = 98.2%

Table 18 Response table for means of SR

Level	C_p	I_p	T_{on}	DC	V_g
1	5.750	3.070	4.478	4.624	4.102
2	3.708	4.477	4.564	4.391	4.543
3	4.331	6.242	4.747	4.773	5.143
Delta	2.042	3.172	0.269	0.382	1.041
Rank	2	1	5	4	3

RLT being lower-the-better type of quality characteristic, the tendency of deviation of the response curves as shown in Fig. 13, demonstrate that the optimal set of parameters for RLT is the first level of parameters of C_p, first level of I_p, third level of T_{on}, third level of DC and first level of V_g. The response table for all the process parameters is shown in Table 21.

3.3.6 Analysis of Variance for Microhardness

From the main effect plots shown in Fig. 14, the influence of different factors on the process can be visualized. The significance of the process variables in relation to

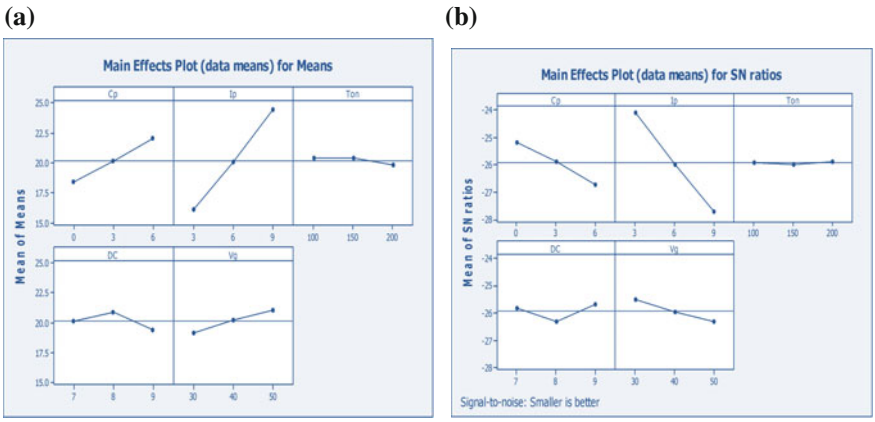

Fig. 13 Main effect plot for means and S/N ratio of recast layer thickness. **a** Main effect plot for means of RLT (Tripathy and Tripathy 2017a). **b** Main effect plot for S/N ratio of RLT

Table 19 ANOVA table for means of RLT

Source	DF	Seq SS	Adj SS	Adj MS	*F*	*P*	*P* (%)
C_p	2	58.191	58.191	29.095	66.13	0.000	14.42
I_p	2	309.912	309.912	154.956	352.20	0.000	76.81
T_{on}	2	2.286	2.286	1.143	2.60	0.105	5.26
DC	2	10.323	10.323	5.161	11.73	0.001	2.55
V_g	2	15.708	15.708	7.854	17.85	0.000	3.89
Error	16	7.039	7.039	0.440			
Total	26	403.459					

S = 0.6633, R-Sq = 98.3%, R-Sq(adj) = 97.2%

Table 20 ANOVA table for S/N ratio of RLT

Source	DF	Seq SS	Adj SS	Adj MS	*F*	*P*	*P* (%)
C_p	2	10.8879	10.8879	5.4439	61.61	0.000	14.19
I_p	2	59.2309	59.2309	29.6154	335.16	0.000	77.28
T_{on}	2	0.0459	0.0459	0.0229	0.26	0.774	0.059
DC	2	2.1335	2.1335	1.0668	12.07	0.001	2.78
V_g	2	2.9230	2.9230	1.4615	16.54	0.000	3.81
Error	16	1.4138	1.4138	0.0884			
Total	26	76.6349					

S = 0.2973, R-Sq = 98.2%, R-Sq(adj) = 97.0%

Table 21 Response table for means of RLT

Level	C_p	I_p	T_{on}	DC	V_g
1	18.40	16.09	20.34	20.13	19.20
2	20.10	20.01	20.40	20.94	20.22
3	21.99	24.39	19.75	19.43	21.07
Delta	3.59	8.29	0.65	1.51	1.87
Rank	2	1	5	4	3

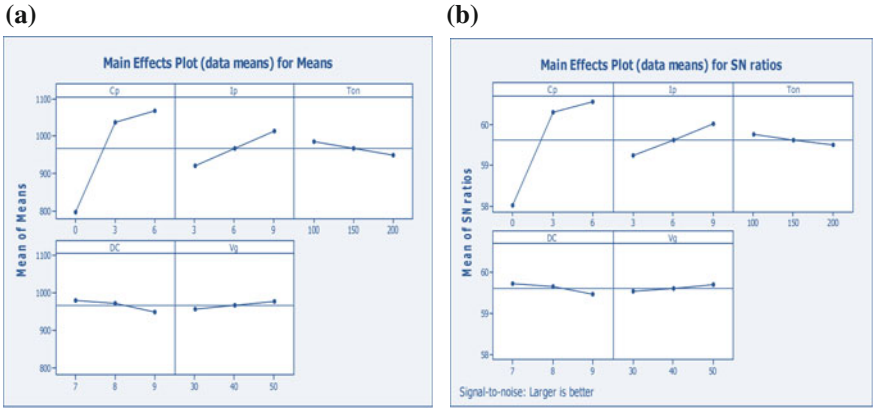

Fig. 14 Main effect plot for means and S/N ratio of microhardness. **a** Main effect plot for means of HVN. **b** Main effect plot for S/N ratio of HVN

HVN has been investigated and the optimum combination of parameters was determined from the ANOVA analysis presented in Tables 22 and 23 respectively.

HVN being higher-the-better type of quality characteristic, the tendency of deviation of the response curves as shown in Fig. 14, demonstrate that the optimal setting of parameters for HVN is the third level of parameters of C_p, third level of I_p, first level of T_{on}, first level of DC and third level of V_g. The response table for all the process parameters is shown in Table 24.

3.4 Multi-objective Optimization Using TOPSIS

The normalized matrix, weighted normalized decision matrix, separation of alternatives from positive and negative ideal solutions and preference values for TOPSIS obtained for experimental runs with ranks are represented in Tables 25, 26, 27 and 28 respectively. The weights given to different parameters are MRR, TWR and SR = 0.2, EWR = 0.1, RLT and HVN = 0.15 (Sum = 1).

It may be observed that the experimental run #21 has the most suitable multiple performance characteristics having the highest preference order followed by #20

Table 22 ANOVA table for means of HVN

Source	DF	Seq SS	Adj SS	Adj MS	*F*	*P*	*P* (%)
C_p	2	395,513	395,513	197,756	636.42	0.000	87.73
I_p	2	38,012	38,012	19,006	61.16	0.000	8.431
T_{on}	2	5551	5551	2776	8.93	0.002	12.11
DC	2	4885	4885	2442	7.86	0.004	1.08
V_g	2	1888	1888	944	3.04	0.076	0.418
Error	16	4972	4972	311			
Total	26	450,821					

S = 17.63, R-Sq = 98.9%, R-Sq(adj) = 98.2%

Table 23 ANOVA table for S/N ratio of HVN

Source	DF	Seq SS	Adj SS	Adj MS	*F*	*P*	*P* (%)
C_p	2	34.9657	34.9657	17.4829	825.92	0.000	90.13
I_p	2	2.7475	2.7475	1.3737	64.90	0.000	7.082
T_{on}	2	0.3203	0.3203	0.1601	7.56	0.005	0.825
DC	2	0.2922	0.2922	0.1461	6.90	0.007	0.753
V_g	2	0.1285	0.1285	0.0642	3.03	0.076	0.331
Error	16	0.3387	0.3387	0.0212			
Total	26	38.7929					

S = 0.1455, R-Sq = 99.1%, R-Sq(adj) = 98.6%

Table 24 Response table for means of HVN

Level	C_p	I_p	T_{on}	DC	V_g
1	796.3	921.1	984.3	980.4	956.7
2	1035.8	965.4	966.0	970.8	965.8
3	1067.4	1013.0	949.2	948.3	977.1
Delta	271.1	91.9	35.1	32.1	20.4
Rank	1	2	3	4	5

and #19. The higher preference values are considered as optimum, therefore, considering the preference values as higher-the-better type of quality characteristic, the third level of parameters of C_p, first level of I_p, third level of T_{on}, second level of DC and third level of V_g offer maximum grades and are considered to be the optimum set of process parameters. The optimal parametric combination is $C_{p3}I_{p1}T_{on3}\mathrm{DC}_2V_{g3}$.

Table 25 Normalized matrix

Run	MRR	TWR	EWR	SR	RLT	HVN
1	0.0581	0.0182	0.0730	0.1498	0.1293	0.1547
2	0.0601	0.0205	0.0798	0.1616	0.1349	0.1535
3	0.0620	0.0237	0.0893	0.1773	0.1424	0.1551
4	0.1027	0.0292	0.0664	0.1919	0.1758	0.1569
5	0.1241	0.0324	0.0610	0.2148	0.1803	0.1586
6	0.1512	0.0387	0.0598	0.2310	0.1852	0.1574
7	0.2133	0.4115	0.4502	0.2562	0.1929	0.1596
8	0.2327	0.5144	0.5159	0.2944	0.2024	0.1582
9	0.2482	0.5539	0.5209	0.3626	0.2084	0.1600
10	0.0708	0.0182	0.0600	0.0764	0.1475	0.1896
11	0.0836	0.0260	0.0728	0.0890	0.1424	0.1951
12	0.0984	0.0199	0.0472	0.1095	0.1466	0.1904
13	0.1466	0.0652	0.1038	0.1430	0.1712	0.2003
14	0.1643	0.0481	0.0684	0.1383	0.1861	0.2076
15	0.1719	0.0670	0.0910	0.1639	0.191	0.2026
16	0.1744	0.1002	0.1341	0.1742	0.2268	0.2121
17	0.2371	0.1435	0.1413	0.1978	0.2359	0.2182
18	0.2693	0.1602	0.1388	0.2227	0.248	0.2234
19	0.1470	0.0280	0.0445	0.095	0.1537	0.1945
20	0.1736	0.0296	0.0399	0.1088	0.1773	0.1997
21	0.1825	0.0282	0.0360	0.1214	0.1831	0.203
22	0.2141	0.0984	0.1073	0.1470	0.1804	0.2088
23	0.2234	0.1580	0.1650	0.1659	0.1988	0.204
24	0.2644	0.1339	0.1182	0.1919	0.2189	0.2182
25	0.2900	0.1972	0.1587	0.2215	0.2420	0.2224
26	0.2978	0.1742	0.1365	0.2408	0.2475	0.22
27	0.3103	0.2473	0.186	0.244	0.2532	0.2249

3.4.1 Confirmatory Experiment for TOPSIS

After the evaluation of optimal parameter setting, prediction and confirmation for the enhancement of quality characteristic using the optimal setting has been examined. The results have been presented in Table 29.

Table 29 shows that the optimum set of parameters obtained from TOPSIS gives an increased MRR with a rise in the value from 2.564 to 9.6 mm^3/min. For this subsequent rise in MRR, the TWR exhibits an increase from a value of 0.0172–0.0395 mm^3/min. The EWR value decreases from 0.6718 to 0.4115%. The surface roughness increases from 3.8 to 4 μm as more amount of material removal leads to the formation of rough surfaces. The recast layer thickness reduces from 13.8 to 13.2 μm and the microhardness value shows an increase from 784 to 1105

Table 26 Weighted normalized decision matrix

Run	MRR	TWR	EWR	SR	RLT	HVN
1	0.0116	0.0036	0.0073	0.0299	0.0194	0.0232
2	0.012	0.0041	0.0079	0.0323	0.0202	0.023
3	0.0124	0.0047	0.0089	0.0354	0.0213	0.0232
4	0.0205	0.0058	0.0066	0.0383	0.0263	0.0235
5	0.0248	0.0064	0.0061	0.0429	0.0270	0.0238
6	0.0302	0.0077	0.0059	0.0462	0.0277	0.0236
7	0.0426	0.0823	0.04502	0.0512	0.0289	0.0239
8	0.0465	0.1028	0.0515	0.0588	0.0303	0.0237
9	0.0496	0.1107	0.05209	0.0725	0.0312	0.024
10	0.0141	0.0036	0.0060	0.0152	0.0221	0.0284
11	0.0167	0.0052	0.0073	0.0178	0.0213	0.02927
12	0.0196	0.0039	0.00472	0.0219	0.022	0.02856
13	0.0293	0.013	0.0104	0.0286	0.0256	0.03004
14	0.0328	0.0096	0.0068	0.0276	0.0279	0.0311
15	0.0343	0.0134	0.0091	0.0327	0.0286	0.0304
16	0.0348	0.02005	0.01341	0.0348	0.034	0.0318
17	0.0474	0.0287	0.01413	0.0395	0.0353	0.0327
18	0.0538	0.03205	0.0138	0.0445	0.0372	0.0335
19	0.0294	0.0056	0.0044	0.0190	0.023	0.0292
20	0.0347	0.0059	0.0039	0.0217	0.0266	0.0299
21	0.0365	0.0056	0.0036	0.0242	0.0274	0.0305
22	0.0428	0.0196	0.0107	0.0294	0.027	0.0313
23	0.0446	0.0316	0.0165	0.0332	0.0298	0.0306
24	0.0528	0.0267	0.0118	0.0383	0.0328	0.0327
25	0.058	0.0394	0.0158	0.0443	0.0363	0.0334
26	0.0595	0.0348	0.0136	0.0481	0.037133	0.033
27	0.062	0.0494	0.0186	0.0488	0.03799	0.03375

by adding graphite powder. The concentration of graphite powder causing more amount of material removal is 6 g/L. The improvement in preference value for ideal solution = 0.1021.

3.4.2 ANOVA for TOPSIS

The influence of process parameters on performance characteristics may be determined by ANOVA. The result for preference solution using ANOVA is given in Table 30. The results of factor responses are considered by using higher-the-better criteria by means of MINITAB software. Table 31 indicates that C_p, I_p, T_{on} and DC are parameters which have a significant contribution towards improvement in the value of preference solution while the role of V_g is insignificant.

Table 27 Separation of alternatives from positive and negative ideal solutions

Run	S^+	S^-
1	0.0537	0.1251
2	0.0541	0.1235
3	0.0549	0.1215
4	0.04923	0.1202
5	0.04821	0.119
6	0.0465	0.1179
7	0.0988	0.0486
8	0.1205	0.0391
9	0.1323	0.0386
10	0.0484	0.1310
11	0.04584	0.1284
12	0.04329	0.1287
13	0.0379	0.1172
14	0.0336	0.1221
15	0.0359	0.1165
16	0.0413	0.1086
17	0.0424	0.1032
18	0.0464	0.1017
19	0.0334	0.1295
20	0.0293	0.1288
21	0.0285	0.1285
22	0.0307	0.1141
23	0.0411	0.1015
24	0.0375	0.1080
25	0.0507	0.0972
26	0.0498	0.1011
27	0.0616	0.0900

The response table for all the process parameters is shown in Table 31. The table demonstrates the ranks based upon the delta statistics which compare the relative magnitude of effects.

3.5 Microstructure Analysis

The SR has been observed to be dependent on the recast layer distribution. The existing thermal conditions damage the surface and make it irregular. The mechanism of melting and mixing of powder in proper concentrations vary the surface properties of the material resulting in its modification. The presence of foreign particles if added in appropriate quantities reduces the SR of the machined parts. Figure 15a, b represent the microstructures obtained at the optimum set of process

Table 28 Estimation of preference value with rank order

Run	Preference value	Order
1	0.6997	18
2	0.6954	19
3	0.6887	20
4	0.7096	16
5	0.7117	14
6	0.7171	15
7	0.3297	25
8	0.2449	26
9	0.2260	27
10	0.7306	11
11	0.737	10
12	0.7483	8
13	0.7557	7
14	0.7841	5
15	0.764	6
16	0.7245	12
17	0.7086	17
18	0.6867	21
19	0.7948	3
20	0.8145	2
21	0.81835	1
22	0.7881	4
23	0.7118	13
24	0.7425	9
25	0.6570	23
26	0.6704	22
27	0.5938	24

parameters with the addition of graphite powder to the dielectric fluid. The surface quality of the machined sample tends to improve as the recast layer thickness and microcracks formation reduce in comparison to machining without the addition of powder. The increase in plasma flushing efficiency during PMEDM results in the ejection of molten material and resolidification. Under constant flushing pressure, with the increase in C_p the SR increases. This is due to the formation of carbide layers resulting from the increased level of carbon from the graphite powder particles. The experimental findings depict that adding powder reduces the SR to a huge extent, but multi-objective optimization helps to determine the most suitable set of parameters with simultaneous optimization of chosen parameters to resulting in improved surface properties of the machined surface.

Table 29 Results of confirmatory experiment

Initial factor setting		Optimal condition
		Experimental
Level	$C_{p1}I_{p1}T_{on1}DC_1V_{g1}$	$C_{p3}I_{p1}T_{on3}DC_2V_{g3}$
Concentration of graphite powder (g/L)	0	6
Peak current (A)	3	3
Pulse on time (μs)	100	200
Duty cycle (%)	7	8
Gap voltage (V)	30	50
MRR (mm^3/min)	2.564	9.6
TWR(mm^3/min)	0.0172	0.0395
EWR (%)	0.6718	0.4115
SR (μm)	3.8	4
RLT(μm)	13.8	13.2
HVN	784	1105
Value of preferred solution	0.732	0.8341

Improvement in preference value for ideal solution = 0.1021

Table 30 ANOVA table for preference solution

Source	DF	Seq SS	Adj SS	Adj MS	F	P	P (%)
C_p	2	0.188	0.1880	0.0940	127.55	0.000	29.67
I_p	2	0.2575	0.2575	0.1287	174.71	0.000	40.64
T_{on}	2	0.0524	0.0524	0.0262	35.60	0.000	8.28
DC	2	0.1215	0.1215	0.0607	82.43	0.000	19.17
V_g	2	0.0023	0.0023	0.0012	1.58	0.237	0.366
Residual error	16	0.0117	0.0118	0.0007			
Total	26	0.6337					

S = 0.02715, R-Sq = 98.1%, R-Sq(adj) = 97.0%

Table 31 Response table for means of preference value

Level	C_p	I_p	T_{on}	DC	V_g
1	0.5581	0.7475	0.7162	0.7009	0.6877
2	0.7377	0.7427	0.6973	0.7429	0.6753
3	0.7323	0.5379	0.6146	0.5843	0.6650
Delta	0.1797	0.2095	0.1016	0.1586	0.0227
Rank	2	1	4	3	5

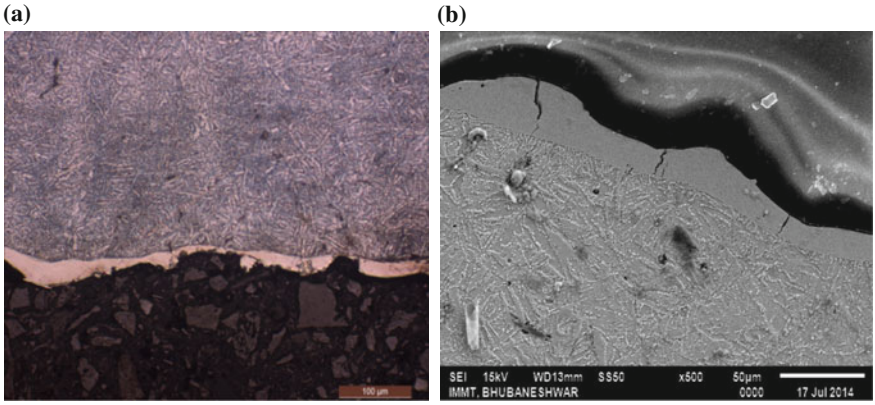

Fig. 15 SEM of surfaces and sub-surfaces for the machining with graphite powder-mixed dielectric. **a** Optical microscopy image of recast layer. **b** SEM micrograph of recast layer

4 Conclusion

The present investigation aims to determine the optimal setting for the process variables to increase the MRR and HVN and minimize the TWR, EWR, SR and RLT simultaneously for H-11 hot work tool steel by adding graphite powder to the dielectric fluid. Taguchi's technique has been implemented to perform the experiments by altering C_p, I_p, T_{on}, DC and V_g. Single-objective optimization has been carried out and an optimum set of process parameters have been identified for the response parameters. Further, multi-objective optimization has been performed using TOPSIS to identify the optimum set of input parameters that improve the process performance. The findings from the present work are as follows:

1. Maximum MRR can be achieved at $\boldsymbol{C_{p3}I_{p3}T_{on3}DC_2V_{g3}}$ when machined using PMEDM. I_p, powder concentration, V_g and T_{on} are the parameters which have significant contribution toward improvement in MRR while the role of DC is insignificant.
2. Minimum TWR can be obtained at $\boldsymbol{C_{p2}I_{p1}T_{on2}DC_2V_{g1}}$. Parameters which have significant contribution toward improvement in TWR are C_p, I_p, T_{on} and DC are while the role of V_g is insignificant.
3. $\boldsymbol{C_{p2}I_{p1}T_{on2}DC_2V_{g1}}$ offer minimum EWR when machined using PMEDM. C_p, I_p, T_{on} and DC are parameters which have significant contribution toward improvement in EWR while the role of V_g is insignificant.
4. Minimum SR is obtained at $\boldsymbol{C_{p2}I_{p1}T_{on1}DC_2V_{g1}}$. Parameters which have a significant contribution towards improvement in SR are C_p, I_p and V_g are while the role of T_{on} and DC is insignificant.

5. Minimum RLT is obtained at $\boldsymbol{C_{p1}I_{p1}T_{on3}DC_3V_{g1}}$. Parameters which have significant contribution towards improvement in RLT is C_p, I_p and V_g are while the role of T_{on} is insignificant.
6. Maximum HVN can be achieved at $\boldsymbol{C_{p3}I_{p3}T_{on1}DC_1V_{g3}}$ when machined using PMEDM. I_p, powder concentration, DC and T_{on} are the parameters which have significant contribution toward improvement in HVN while the role of V_g is insignificant.
7. The multi-objective optimization results show that C_p of 6 g/L, I_p of 3 A, T_{on} of 200 μs, DC of 80% and V_g of 50 V i.e. $\boldsymbol{C_{p3}I_{p1}T_{on3}DC_2V_{g3}}$ is the optimal setting using TOPSIS. The optimal setting obtained can develop the performance of the quality characteristics under consideration.
8. Confirmatory test shows improvement of 0.1021 in the preferred values for the optimum set using TOPSIS as compared to the initial setting, which is satisfactory.
9. The significant machining parameters affecting the process characteristics at 95% confidence interval were determined using ANOVA. The adjusted R^2 value was found to be 98.1% which means that 98.1% of the response variables fit the linear model.
10. The microstructure analysis was done for the optimal setting which shows improved properties due to less crack formation, lower roughness values and small thickness of recast layer.
11. The model is appropriate for use to identify the most suitable set of input parameters for the required performance characteristics. The outcome of the present research work will be a substantial aid to the industries concerned with the use of materials processed through PMEDM.
12. Adding powder particles to the dielectric widens the gap, improves the flushing and makes the process stable. However, powders should be added in appropriate concentrations as they tend to settle down in the tank and cause difficulty in stirring.

References

Assarzadeh, S., and M. Ghoreishi. 2013. A dual response surface-desirability approach to process modeling and optimization of Al_2O_3 powder-mixed electric discharge machining (PMEDM) parameters. *International Journal of Advanced Manufacturing Technology* 64: 1459–1477.

Batish, A., and A. Bhattacharya. 2012. Mechanism of material deposition from powder, electrode and dielectric for surface modification of H-11 and H-13 die steels in EDM process. *Materials Science Forum* 701: 61–75.

Gadakh, V.S. 2012. Parametric optimization of wire electric discharge machining using TOPSIS method. *Advances in Production Engineering & Management* 7 (4): 157–164.

Kumar, S., R. Singh, T.P. Singh, and B.L. Sethi. 2009. Surface modification by electrical discharge machining: A review. *Journal of Materials Processing Technology* 209: 3675–3687.

Lal, Shyam, Sudhir Kumar, Zahid A. Khan, and Arshad N. Siddiquee. 2015. Multi-response optimization of wire electrical discharge machining process parameters for Al7075/$Al2O_3$/SiC hybrid composite using Taguchi-based grey relational analysis. *Journal of Engineering Manufacture* 1–9.

Pecas, P., and E. Henriques. 2008. Electrical discharge machining using simple and powder mixed dielectric: The effect of the electrode area on the surface roughness and topography. *Journal of Materials Processing Technology* 200: 250–258.

Sidhu, Sarabjeet Singh, Ajay Batish, and Sanjeev Kumar. 2014. ED Machining of Particulate Reinforced MMC's. *International Journal of Mechanical, Aerospace, Industrial, Mechatronics and Manufacturing Engineering* 8(3):509–515.

Singh, Baljinder, Paramjit Singh, Gaurav Tejpal, and Singh Gurtej. 2012. An experimental study of surface roughness of H-11 in EDM process using copper tool electrode. *International Journal of Advanced Manufacturing Technology* 3 (4): 30–33.

Singh, A.K., S. Kumar, and V.P. Singh. 2015. Effect of the addition of conductive powder in dielectric on the surface properties of superalloy Super Co 605 by EDM process. *International Journal of Advanced Manufacturing Technology* 77: 99–106.

Talla, Gangadharudu, Deepak Kumar Sahoo, S. Gangopadhyay, and C. K. Biswas. 2015. Modeling and multi-objective optimization of powder mixed electric discharge machining process of aluminium/alumina metal matrix composite. *Engineering Science and Technology* 1–5.

Tripathy, S., and D.K. Tripathy. 2016. Multi-attribute optimization of machining process parameters in powder mixed electro-discharge machining using TOPSIS and grey relational analysis. *Engineering Science and Technology: an International Journal* 19 (1): 62–70.

Tripathy, S., and D.K. Tripathy. 2017a. Multi-response optimization of machining process parameters for powder mixed electro-discharge machining using grey relational analysis and topsis. *Machining Science and Technology* 21 (3): 362–384.

Tripathy, S., and D.K. Tripathy. 2017b. Optimization of process parameters and investigation on surface characteristics during EDM and powder mixed EDM.' In *Innovative design and development practices in Aerospace and Automotive Engineering*, eds. R. Bajpai, and U. Chandrasekhar, Lecture notes in Mechanical Engineering, pp. 385–391. Singapore: Springer.

Tripathy, S., and D.K. Tripathy. 2017c. Grey Relational Analysis and its application on surface properties during EDM and Powder Mixed EDM. *Journal of Engineering Science and Technology* 12 (9): 2374–2392.